Available online at www.sciencedirect.com
SCIENCE DIRECT®
Journal of Sound and Vibration 286 (2005) 207–228
JOURNAL OF SOUND AND VIBRATION
www.elsevier.com/locate/jsvi

The transient dynamics of multiple accelerating/decelerating masses traveling on an initially curved beam

Yi-Ming Wang

Department of Mechatronics Engineering, College of Engineering, National Chunghua Normal University, Chunghua, 500, Taiwan

Received 22 June 2004; received in revised form 14 September 2004; accepted 1 October 2004
Available online 23 December 2004

Abstract

The objective of this paper is an analytical and numerical study of the transient dynamics of a beam–mass system carrying multiple masses moving along an initially curved beam. An attention is given to the phenomena arising due to the initial curvature, initial imperfection, of a beam and the motion produced by the existence of multiple moving masses.

The method used in the analysis is Newtonian. The mechanics of the interface between the masses and the beam is determined by modeling the masses as rigid bodies that are rolling on an initially curved flexible structure when the moving masses are set on motion. Based on the Euler–Bernoulli beam theory, the mechanics, including effects due to friction and convective accelerations, of the interfaces between the moving masses and the beam are obtained.

Result of present study shows that the initial curvature of a beam can result significant effects to the dynamics of the system even if the initial imperfection of the beam is small. The magnification of the amplitude of response of the system due to the initial deviation of beam depends on the initial speed of mass, the applied forward/retard force on the mass, and the friction between the mass and the beam.

E-mail address: wangym@cc.ncue.edu.tw (Y.-M. Wang).

0022-460X/$ - see front matter © 2004 Elsevier Ltd. All rights reserved.
doi:10.1016/j.jsv.2004.10.036

1. Introduction

Vibrations of flexible structures with attached moving masses have been the subject of many studies [1–13]. Steele [1,2] investigated the response of a simple supported finite beam with and without elastic foundation under a moving load. He pointed out that the existence of a truly critical speed and the impossibility of the occurrence of a steady-state occur when the load speed is equal to either the shear or the bar velocity.

Ting et al. [3] studied the problem regarding the interaction between the moving mass and the supporting structure. They concluded that if "correct" formulation is desired the convective acceleration terms should be included.

An attention is given to the phenomenon produced by the existence of negative displacement of a beam due to the motion of an attached moving mass. Lee [4] investigated the occurrence and relative conditions of the separation between flexible structures and riding masses.

Recently, sophisticated effects, such as longitudinal deflections, inertia, nonlinearity of the flexible structure, the variation of moving masses to the response, and the occurrence of instability of the response have been the subjects of many studies [5–7]. Adams [5] studied the critical speeds and the response of a tensioned beam due to the motion of attached cyclic moving loads. Wang [6] employed the method of multiple time scales to study the growth of small amplitude vibrations into large motion regime of a beam–mass system due to the occurrence of two-component parametric resonance.

Kononov and Borst [7] analyzed the occurrence of instability of the response of four different flexible structures under elastic foundation due to the motion of a riding mass moving with constant velocity. Their result indicated that negative damping might occur when the mass velocity exceeded the smallest phase velocity of the waves in the system. This could cause the solutions became unstable.

Mofid and Shadnam [8] studied the response of beams with internal hinges when a moving mass sliding on it. They examined the transient dynamics of the system due to various boundary conditions.

Wang [9] considered a model that a moving mass may increase or decrease its speed during operation. A single mass moving on a perfect straight beam on a uniform elastic foundation was assumed in the modeling.

Although, the problem of moving mass has been studied by many authors, however, the dynamics of multiple accelerating/decelerating masses rolling on an initially curved beam has not been studied yet. Hence, in this study, the purpose is to present a methodology to evaluate the transient dynamics of a beam–mass system carrying multiple accelerating/decelerating masses riding on a beam with initial curvature, geometric imperfection. Unlike other papers, in which a single mass with either constant velocity or acceleration moving along a perfect straight beam is assumed, in this paper the equations of motion of a beam–mass system carrying multiple traveling masses rolling on an initially curved beam are derived. Various effects, such as the initial deviation of a beam, the initial speed of moving masses, the friction and et al., to the motion of the system are examined.

2. Basic formulas

In this study, multiple moving masses rolling on a finite, simple supported, initially curved beam is considered. The beam rests on a uniform elastic foundation and is of length ℓ and initial

variation $\bar{v}_0(s)$. Here $\bar{v}_0(s)$, $\bar{v}_0(s) = v_0^* \sin \pi s/\ell$, is the initial deviation of the beam measured from straight axis with v_0^* being the amplitude of initial deviation. The static state of the beam is obtained by assuming that the gravity of the beam and the foundation preload are in the state of equilibrium.

From Fig. 1, the equations governing the motion of the system can be derived from the dynamic equilibrium of forces and momenta and are given as

$$\mathbf{F}_{,s} + \sum_{i=1}^{m} \mathbf{f}_i = \bar{m}\mathbf{r}_{,tt}, \quad 0 < s < l, \quad t > 0, \tag{1a}$$

$$\bar{M}_{,s} - V = 0, \tag{1b}$$

$$\bar{M} = -EIv_{,ss}, \tag{1c}$$

with the inextensibility constraint $\mathbf{r}_{,s} \cdot \mathbf{r}_{,s} = 1$. The force $\mathbf{F}$ is given by

$$\begin{aligned} \mathbf{F} &= \mathbf{H}\mathbf{i} + \mathbf{P}\mathbf{j} \\ &= [T\cos(\theta + \theta_0) - V\sin(\theta + \theta_0)]\mathbf{i} + [T\sin(\theta + \theta_0) + V\cos(\theta + \theta_0)]\mathbf{j}. \end{aligned} \tag{1d}$$

In the above equations, $\mathbf{i}$ and $\mathbf{j}$ represent the unit vectors of the coordinate system in the x and y directions, respectively. $\bar{M}$ is the bending moment acting on the element. T and V are the axial and the transverse forces in the beam, respectively. m denotes the number of traveling masses riding on the beam. $\bar{m}$ represents the mass per unit length of the beam. θ_0 and θ indicate the initial angle between the neutral axis of the beam and the x-axis and the dynamic angle from the static state, respectively. E is the Young's modulus and I is the area moment of inertia of the beam. The subscript s and t denote the s and t differentiation. $\mathbf{r}(s, t)$ is the Cartesian position vector of point s along the beam at time t and has the form

$$\mathbf{r}(s, t) = [x(s) + u(s, t)]\mathbf{i} + [v(s, t) + \bar{v}_0(s)]\mathbf{j}, \tag{2}$$

where $u(s, t)$ and $v(s, t)$ are the axial and the transverse displacements of the beam from the undeformed state, respectively.

The force $\mathbf{f}_i$ represents the external forces including the weight and the moving reaction of the ith mass upon the beam and can be stated by

$$\mathbf{f}_i = -kv\mathbf{j} + (N_i\mathbf{n} + \mu N_i\hat{\boldsymbol{\tau}})\bar{\delta}(s - \bar{s}_i(t)), \tag{3}$$

where N_i, $\bar{\delta}(s - \bar{s}_i(t))$, and $\bar{s}_i(t)$ denote the reaction of beam on the ith mass, the Dirac delta function, and the position of the ith mass along the arc of the beam at time t, respectively; μ is the coefficient of friction between the mass and the beam and k is the foundation stiffness per unit length.

The equation of motion of the ith mass obeys (Fig. 1)

$$M_i\mathbf{a}_M^i = M_i\mathbf{g} + \mathbf{f}_M^i - \mu N_i\hat{\boldsymbol{\tau}} - N_i\mathbf{n}, \tag{4}$$

where $M_i =$ the mass of the ith moving mass, $\hat{\boldsymbol{\tau}} = \cos(\theta + \theta_0)\mathbf{i} + \sin(\theta + \theta_0)\mathbf{j} \approx [(1 + u_{,s}) - v_{,s}\bar{v}_{0,s}]\mathbf{i} + (v_{,s} + \bar{v}_{0,s})\mathbf{j}$, $\mathbf{n} = -\sin(\theta + \theta_0)\mathbf{i} + \cos(\theta + \theta_0)\mathbf{j}$, $\mathbf{g} = g\mathbf{j}$. Note that here it is assumed that whenever the ith mass is being driving by a force along the beam, the force on the mass will be

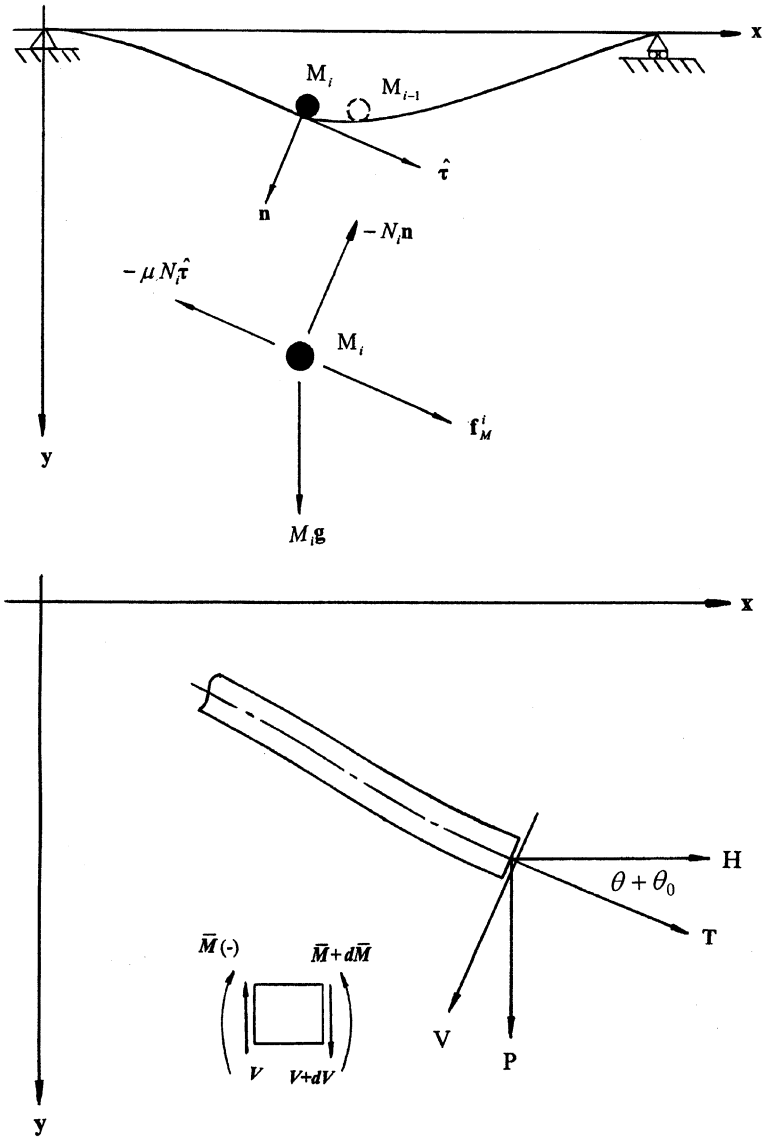

Fig. 1. System configuration and force equilibrium diagram.

along the tangent to the vibrating beam. Hence, $\mathbf{f}_M^i = M_i f_i \hat{\boldsymbol{\tau}}$ and f_i is a prescribed function of time. For example, f_i may be a positive constant to increase the speed or a negative constant to decrease the speed of the ith mass.

The acceleration of the ith moving mass $\mathbf{a}_M^i$ is obtained from

$$\mathbf{a}_M^i = \frac{\mathrm{d}^2}{\mathrm{d}t^2}[\mathbf{r}(\bar{s}_i(t), t)] = \mathbf{r}_{,ss}(\bar{s}_{i,t})^2 + 2\mathbf{r}_{,st}\bar{s}_{i,t} + \mathbf{r}_{,s}\bar{s}_{i,tt} + \mathbf{r}_{,tt}. \tag{5}$$

The corresponding boundary conditions for the finite, simple supported Euler–Bernoulli beam are

$$u(0,t) = v(0,t) = v(\ell,t) = \frac{\partial^2 v(0,t)}{\partial s^2} = \frac{\partial^2 v(\ell,t)}{\partial s^2} = 0, \tag{6}$$

$$H(\ell,t) = T(\ell,t)[(1+u_{,s}) - v_{,s}\bar{v}_{0,s}] + EI\, v_{,sss}(v_{,s} + \bar{v}_{0,s}) = 0, \quad \text{at } s = \ell, \tag{7}$$

where Eq. (7) is obtained under the condition that the resultant in the **i** direction vanished at $s = \ell$.

Introducing the following dimensionless quantities

$$\tau = \sqrt{\frac{EI}{\bar{m}l\ell^4}}\,t,\ \ \hat{M} = \frac{M}{\bar{m}\ell},\ \ \hat{T} = \frac{\ell^2}{EI}\,T,\ \ \hat{f} = \frac{\bar{m}\ell^3}{EI}\,f, \hat{g} = \frac{\bar{m}\ell^3}{EI}\,g,$$

$$\hat{k} = \frac{k\ell^3}{EI},\ \ \eta = \frac{s}{\ell},\ \ \xi_i = \frac{\bar{s}_i}{\ell},\ \ \hat{v} = \frac{v}{\ell},\ \ \hat{u} = \frac{u}{\ell},\ \ \hat{\bar{v}}_0 = \frac{\bar{v}_0}{\ell}, \tag{8}$$

and substituting Eqs. (1b)–(8) with the inextensibility constraint into Eq. (1a), the equation of motion of the combined system in directions **i** and **j** yields, in dimensionless form,

$$\begin{aligned}
&\{\hat{T}[(1+\hat{u}') - \hat{v}'\hat{\bar{v}}_0'] + \hat{v}'''(\hat{v}' + \hat{\bar{v}}_0')\}' + \sum_{i=1}^{m} \hat{M}_i\hat{f}_i[(1+\hat{u}') - \hat{v}'\hat{\bar{v}}_0'])\delta(\eta - \xi_i) \\
&\quad = \ddot{\hat{u}} + \sum_{i=1}^{m} \hat{M}_i\{[\hat{u}'' - (\hat{v}'\hat{\bar{v}}_0')'](\dot{\xi}_i)^2 + 2(\dot{\hat{u}}' - \dot{\hat{v}}'\hat{\bar{v}}_0')\dot{\xi}_i \\
&\qquad + [(1+\hat{u}') - \hat{v}'\hat{\bar{v}}_0'][\ddot{\xi}_i + \ddot{\hat{u}}]\delta(\eta - \xi_i), \quad 0 < \eta < 1,\ \tau > 0,
\end{aligned} \tag{9a}$$

$$\begin{aligned}
&\{\hat{T}(\hat{v}' + \hat{\bar{v}}_0') - \hat{v}'''[(1+\hat{u}') - \hat{v}'\hat{\bar{v}}_0']\}' + \sum_{i=1}^{m} \hat{M}_i[\hat{f}_i(\hat{v}' + \hat{\bar{v}}_0') + \hat{g}]\delta(\eta - \xi_i) \\
&\quad = \ddot{\hat{v}} + \hat{k}\hat{v} + \sum_{i=1}^{m} \hat{M}_i[(\hat{v}'' + \hat{\bar{v}}_0'')(\dot{\xi}_i)^2 + 2\dot{\hat{v}}'\dot{\xi}_i + (\hat{v}' + \hat{\bar{v}}_0')\ddot{\xi}_i + \ddot{\hat{v}}]\delta(\eta - \xi_i), \\
&\quad 0 < \eta < 1, \tau > 0,
\end{aligned} \tag{9b}$$

where a superposed prime and a dot denote the η and τ differentiation and $\hat{\bar{v}}_0 = \bar{v}_0/\ell = v_0^*/\ell \sin \pi\eta \equiv v_0 \sin \pi\eta$.

Considering small deformations and assuming that the variation of axial force is to remain continuous at $\eta = \xi_i(\tau), i = 1, 2, \ldots$, the axial force $\hat{T}$ can first be determined by integrating Eq. (9a) and using the boundary condition, Eq. (7). This result then is inserted into Eq. (9b). After manipulating these equations and neglecting nonlinear terms in the displacement field when compare these terms to the linear term of $\hat{v}(\eta,\tau)$ and unity, Eq. (9b) yields

$$\begin{aligned}
&\ddot{\hat{v}} + \hat{v}'''' + \hat{k}\hat{v} + \sum_{i=1}^{m} \hat{M}_i\{(\hat{v}'' + \hat{\bar{v}}_0'')(\dot{\xi}_i)^2 + 2\dot{\hat{v}}'\dot{\xi}_i + (\hat{v}' + \hat{\bar{v}}_0')\ddot{\xi}_i \\
&\qquad + \ddot{\hat{v}} - [\hat{f}_i(\hat{v}' + \hat{\bar{v}}_0') + \hat{g}]\}\delta(\eta - \xi_i), \quad 0 < \eta < 1,\ \tau > 0.
\end{aligned} \tag{10}$$

Similarly, considering the equation of motion of the ith mass, Eq. (4), one has

$$\ddot{\xi}_i - [\mu(\hat{v}'' + \hat{\bar{v}}_0'')(\dot{\xi}_i)^2 - 2\mu\dot{\hat{v}}'\dot{\xi}_i = \hat{f} - \hat{g}[\mu - (\hat{v}' + \hat{\bar{v}}_0')] + \mu\ddot{\hat{v}}, \quad \eta = \xi_i,\ \tau > 0. \tag{11}$$

Note that Eq. (11) was obtained by eliminating the normal reaction force N_i of beam on the ith mass between the two equations in directions **i** and **j** of Eq. (4) and using the inextensibility constraint. Therefore, Eqs. (9a), (9b), (10) and (11) with the inextensibility constraint account for $\hat{u}(\eta,\tau)$, $\hat{v}(\eta,\tau)$, $\hat{T}$ and ξ_i when $\hat{M}_i$, μ, $\hat{g}$, $\hat{\bar{v}}_0$, and the boundary conditions, Eqs. (6) and (7), are specified. Hence, examination of the transient dynamics governed by Eqs. (10) and (11) is the main purpose in this study.

By representing $\hat{v}$ as a continuous function and letting $\hat{v} = \sum_{n=1}^{\infty} A_n(\tau)\sin n\pi\eta$, $0<\eta<1, \tau>0$, the boundary condition, Eq. (6), then is satisfied. The approximate solution of the beam–mass system can be obtained by employing the Galerkin's method. Using Galerkin's procedure for removal of spatial dependence, Eq. (10) is multiplied by $\sin j\pi\eta$ and then it is integrated with respect to η from zero to one. The approximate solutions of the beam–mass system carrying multiple traveling masses are given as

$$\begin{aligned}
&\ddot{A}_j(\tau) + \omega_j^2 A_j(\tau) + 2\sum_{i=1}^{m}\hat{M}_i\sum_{n=1}^{\infty}\{(\ddot{\xi}_i - \hat{f}_i)R_{ijn}(\xi_i)A_n(\tau) - (\dot{\xi}_i)^2 S_{ijn}(\xi_i)A_n(\tau)\\
&\quad + 2\dot{\xi}_i R_{ijn}(\xi_i)\dot{A}_n(\tau) + \hat{S}_{ijn}(\xi_i)\ddot{A}_n(\tau)\}\\
&\qquad = 2\sum_{i=1}^{m}\hat{M}_i[\hat{g}\hat{S}_{ij}(\xi_i) - (\ddot{\xi}_i - \hat{f}_i)R_{ij1}(\xi_i)v_0 + (\dot{\xi}_i)^2 S_{ij1}(\xi_i)v_0], \quad 0<\eta<1,\ \tau>0.
\end{aligned} \tag{12}$$

Also the equation of motion of the ith mass, Eq. (11), becomes

$$\begin{aligned}
&\ddot{\xi}_i + \mu\left[\sum_{n=1}^{\infty} S_{in}(\xi_i)A_n(\tau) + S_{i1}(\xi_i)v_0\right](\dot{\xi}_i)^2 - 2\mu\sum_{n=1}^{\infty} C_{in}(\xi_i)\dot{A}_n(\tau)\dot{\xi}_i\\
&\qquad = (\hat{f}_i - \mu\hat{g}) + \hat{g}\left[\sum_{n=1}^{\infty} C_{in}(\xi_i)A_n(\tau) + C_{i1}(\xi_i)v_0\right] + \mu\sum_{n=1}^{\infty}\hat{S}_{in}(\xi_i)\ddot{A}_n(\tau), \quad \tau>0,
\end{aligned} \tag{13}$$

where

$$\omega_j^2 = [(j\pi)^4 + \hat{k}],$$

$$v_0 = \frac{v_0^*}{\ell},$$

$$R_{ijn}(\xi_i) = (n\pi)\sin j\pi\xi_i \cos n\pi\xi_i,$$

$$\hat{S}_{ijn}(\xi_i) = \sin j\pi\xi_i \sin n\pi\xi_i,$$

$$S_{ijn}(\xi_i) = (n\pi)^2\hat{S}_{ijn}(\xi_i),$$

$$\hat{S}_{in}(\xi_i) = \sin n\pi\xi_i,$$

$$C_{in}(\xi_i) = (n\pi)\cos n\pi\xi_i.$$

To write the equations of motion in matrix form, it allows the parameters j and n in Eqs. (12) and (13) to have the range

$$j = 1, 2, 3, \ldots, N,$$
$$n = 1, 2, 3, \ldots, N,$$

and let

$$\mathbf{y} = (A_1, A_2, \ldots, A_N)^{\mathrm{T}}. \tag{14}$$

Then Eq. (12) can be written as

$$\mathbf{M}(\xi_i)\ddot{\mathbf{y}}(\tau) + \sum_{i=1}^{m} \dot{\xi}_i \mathbf{N}_i(\xi)\dot{\mathbf{y}}(\tau) + \mathbf{K}_1(\xi_i)\mathbf{y} + \sum_{i=1}^{m} \ddot{\xi}_i \mathbf{K}_{2i}(\xi_i)\mathbf{y} + \sum_{i=1}^{m} \dot{\xi}_i^2 \mathbf{K}_{3i}(\xi_i)\mathbf{y} + \sum_{i=1}^{m} \ddot{\xi}_i \tilde{\mathbf{c}}_i + \sum_{i=1}^{m} \dot{\xi}_i^2 \tilde{\mathbf{s}}_i = \mathbf{h}(\xi_i) \tag{15}$$

and Eq. (13) is given as

$$\ddot{\xi}_i + [p_i(\xi_i, \mathbf{y}) + \bar{p}_i(\xi_i, v_0)]\dot{\xi}_i^2 + q_i(\xi_i, \dot{\mathbf{y}})\dot{\xi}_i + \mathbf{d}_i^{\mathrm{T}}(\xi_i)\ddot{\mathbf{y}} + \mathbf{e}_i^{\mathrm{T}}(\xi_i)\mathbf{y} = f_i^*. \tag{16}$$

The initial conditions are

$$\dot{\mathbf{y}}(0) = \mathbf{y}(0) = \mathbf{0}, \quad \dot{\xi}_i(0) = \dot{\xi}_i^0 \text{ and } \xi_i(0) = \xi_i^0, \tag{17}$$

where $\dot{\xi}_i^0$ and ξ_i^0 are the initial speed and the position of the ith mass along the beam, respectively. The components of the previously defined matrices, vectors and scalars in Eqs. (15) and (16), i.e., $\mathbf{M}$, $\mathbf{K}_1$, $\mathbf{N}_i$, $\mathbf{K}_{2i}$, $\mathbf{K}_{3i}$, $\tilde{\mathbf{c}}_i$, $\tilde{\mathbf{s}}_i$, $\mathbf{h}$, p_i, $\bar{p}_i$, q_i, $\mathbf{d}_i$, $\mathbf{e}_i$ and f_i^* are given in the appendix.

Now, introducing new state vectors $\mathbf{z}$ into Eqs. (15) and (16) to obtain the numerical integration scheme of the system with the associated initial conditions as specified in Eq. (17), let

$$\mathbf{z} = (\dot{\mathbf{y}}^{\mathrm{T}}, \dot{\boldsymbol{\xi}}^{\mathrm{T}}, \mathbf{y}^{\mathrm{T}}, \boldsymbol{\xi}^{\mathrm{T}})^{\mathrm{T}}, \tag{18}$$

where $\mathbf{z}$ is the $2N + 2m$ vector with $\dot{\boldsymbol{\xi}} = (\dot{\xi}_1, \ldots, \dot{\xi}_i, \ldots, \dot{\xi}_m)^{\mathrm{T}}$ and $\boldsymbol{\xi} = (\xi_1, \ldots, \xi_i, \ldots, \xi_m)^{\mathrm{T}}$. The initial condition of $\mathbf{z}$ in Eq. (18) is $\mathbf{z}(0) = (\mathbf{0}^{\mathrm{T}}, \dot{\boldsymbol{\xi}}_0^{\mathrm{T}}, \mathbf{0}^{\mathrm{T}}, \boldsymbol{\xi}_0^{\mathrm{T}})^{\mathrm{T}}$, where $\mathbf{0}$ is $N \times 1$ zero matrix. $\dot{\boldsymbol{\xi}}_0$ and $\boldsymbol{\xi}_0$ are $m \times 1$ initial velocity and position matrices, respectively. Hence, Eqs. (15) and (16) can be written as

$$\tilde{\mathbf{M}}\dot{\mathbf{z}} + \tilde{\mathbf{N}}\mathbf{z} + \tilde{\mathbf{f}} = \mathbf{0}. \tag{19}$$

In Eq. (19), $\tilde{\mathbf{M}}$ and $\tilde{\mathbf{N}}$ are $(2N + 2m) \times (2N + \times 2m)$ matrices and $\tilde{\mathbf{f}}$ is the $(2N + 2m)$ vector defined by

$$\tilde{\mathbf{M}} = \begin{bmatrix} \mathbf{M} & \bar{\mathbf{K}}_{2m} & \bar{\mathbf{N}} & [\bar{\mathbf{0}}_m]^{\mathrm{T}} \\ \bar{\mathbf{D}}_m^{\mathrm{T}} & \mathbf{I}_m & [\bar{\mathbf{0}}_m] & \mathbf{I}_{\dot{\xi}p} \\ [\mathbf{0}] & [\bar{\mathbf{0}}_m]^{\mathrm{T}} & \mathbf{I} & [\bar{\mathbf{0}}_m]^{\mathrm{T}} \\ [\bar{\mathbf{0}}_m] & [\mathbf{0}_m] & [\bar{\mathbf{0}}_m] & \mathbf{I}_m \end{bmatrix},$$

$$\tilde{\mathbf{N}} = \begin{bmatrix} [\mathbf{0}] & \bar{\mathbf{S}}_m & \bar{\mathbf{K}} & [\bar{\mathbf{0}}_m]^{\mathrm{T}} \\ [\bar{\mathbf{0}}_m] & \mathbf{I}_q & \bar{\mathbf{E}}_m & [\mathbf{0}_m] \\ -\mathbf{I} & [\bar{\mathbf{0}}_m]^{\mathrm{T}} & [\mathbf{0}] & [\bar{\mathbf{0}}_m]^{\mathrm{T}} \\ [\bar{\mathbf{0}}_m] & -\mathbf{I}_m & [\bar{\mathbf{0}}_m] & [\mathbf{0}_m] \end{bmatrix},$$

$$\tilde{\mathbf{f}} = (-\mathbf{h}^{\mathrm{T}}, -\bar{\mathbf{f}}_m^{\mathrm{T}}, \mathbf{0}^{\mathrm{T}}, \mathbf{0}_m^{\mathrm{T}})^{\mathrm{T}},$$

where $\mathbf{I} = N \times N$ unit matrix, $[\mathbf{0}] = N \times N$ zero matrix, $\mathbf{0} = N \times 1$ zero matrix, $\mathbf{I}_m = m \times m$ unit matrix, $[\bar{\mathbf{0}}_m] = m \times N$ zero matrix, $[\mathbf{0}_m] = m \times m$ zero matrix, and $\mathbf{0}_m = m \times 1$ zero matrix. Other sub-matrices are given as follows:

$$\bar{\mathbf{K}}_{2m} = N \times m \text{ matrix} = [\mathbf{K}_{21}\mathbf{y} + \tilde{\mathbf{c}}_1, \ldots, \mathbf{K}_{2i}\mathbf{y} + \tilde{\mathbf{c}}_i, \ldots, \mathbf{K}_{2m}\mathbf{y} + \tilde{\mathbf{c}}_m],$$

$$\bar{\mathbf{D}}_m = N \times m \text{ matrix} = [\mathbf{d}_1, \ldots, \mathbf{d}_i, \ldots, \mathbf{d}_m],$$

$$\bar{\mathbf{E}}_m = m \times N \text{ matrix} = [\mathbf{e}_1, \ldots, \mathbf{e}_i, \ldots, \mathbf{e}_m]^{\mathrm{T}},$$

$$\mathbf{I}_{\dot{\xi}p} = m \times m \text{ diagonal matrix} = \mathrm{diag}[\dot{\xi}_1(p_1 + \bar{p}_1), \ldots, \dot{\xi}_i(p_i + \bar{p}_i), \ldots, \dot{\xi}_m(p_m + \bar{p}_m)],$$

$$\bar{\mathbf{N}} = N \times N \text{ matrix} = [\mathbf{N}_1, \ldots, \mathbf{N}_i, \ldots, \mathbf{N}_m] \times (\xi_1, \ldots, \xi_i, \ldots, \xi_m)^{\mathrm{T}},$$

$$\bar{\mathbf{K}} = N \times N \text{ matrix} = \mathbf{K}_1 + [\mathbf{K}_{31}, \ldots, \mathbf{K}_{3i}, \ldots, \mathbf{K}_{3m}] \times (\dot{\xi}_1^2, \ldots, \dot{\xi}_i^2, \ldots, \dot{\xi}_m^2)^{\mathrm{T}},$$

$$\bar{\mathbf{S}}_m = N \times m \text{ matrix} = [\dot{\xi}_1\tilde{\mathbf{s}}_1, \ldots, \dot{\xi}_i\tilde{\mathbf{s}}_i, \ldots, \dot{\xi}_m\tilde{\mathbf{s}}_m],$$

$$\mathbf{I}_q = m \times m \text{ diagonal matrix} = \mathrm{diag}[q_1, \ldots, q_i, \ldots, q_m],$$

$$\mathbf{f}_m = m \times 1 \text{ matrix} = (f_1^*, \ldots, f_i^*, \ldots, f_m^*)^{\mathrm{T}}.$$

3. Numerical results and discussions

For studying the transient dynamics produced by the motion of multiple moving masses, the number of moving masses used in the numerical examples is set to be one and two. The transient phenomena generated by more than two moving masses can be obtained by similar ways.

In order to evaluate the influence of initial curvature of the beam to the dynamic response of the system, unless otherwise specified, three small values of dimensionless amplitude of initial curvature of the beam are chosen; they are $v_0 = 0.0$ (initially straight), 0.025, and 0.05. In addition, the quantity $EI/\bar{m}l^4$ is set to be $(9.4/\pi)^2$.

For numerical integration of the system, Eq. (19), the Runge–Kutta method with sixth-order accuracy is used. The accuracy of the model and the dimension N of $\mathbf{z}$ in Eq. (19) that is necessary to retain for sufficient accuracy is shown in Fig. 2. As illustrated in Fig. 2, the accuracy of the model, with an attached single mass, was tested by comparison of its results with the results of Ting et al. [3] (lower plot). The parameters used in this figure are exactly the same as those used in

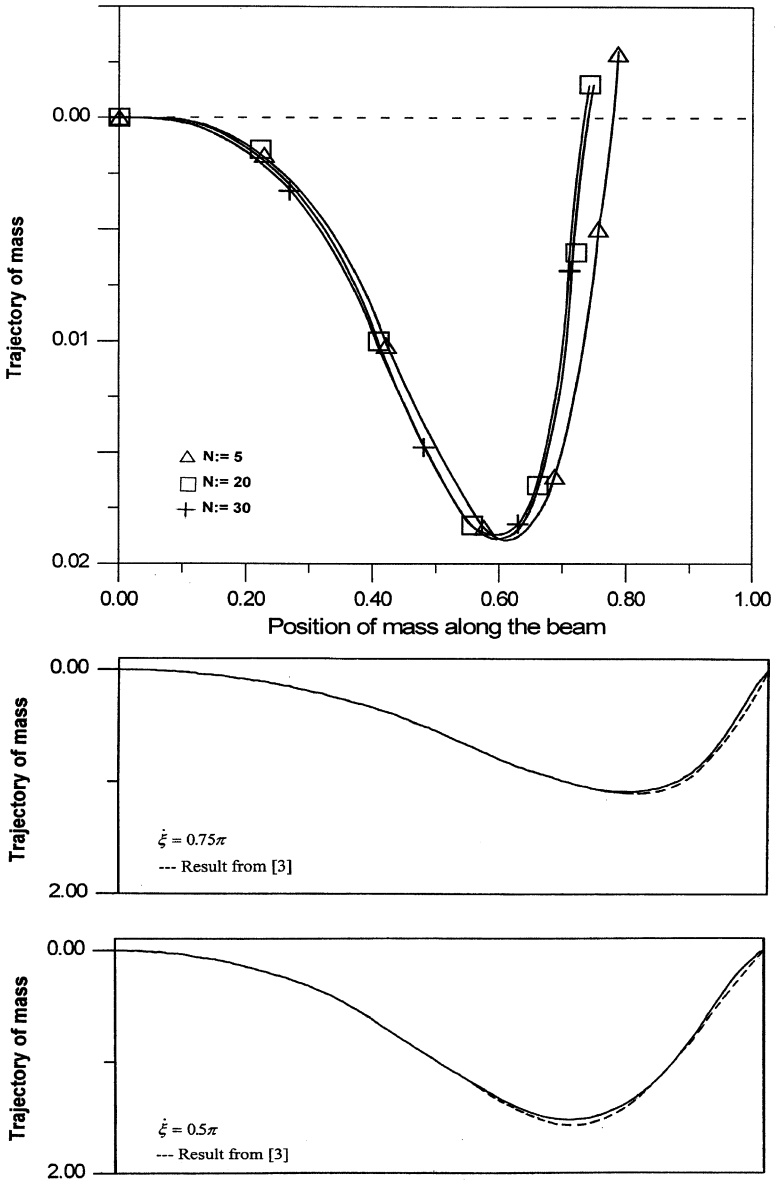

Fig. 2. Rate of convergence of solutions and the trajectory of mass vs. the position of mass along the beam with the same parameters as used in Ref. [3] for $\dot{\xi} = 0.75\pi$ and $\dot{\xi} = 0.5\pi$.

Ting et al. [3]. Those are $\ddot{\xi} = \hat{f} = 0$, $\hat{M} = 0.5$, $\hat{v}_{st} = \hat{M}\hat{g}/48$, and $\dot{\xi} = 0.5\pi$ and $\dot{\xi} = 0.75\pi$. The dimension N of $\mathbf{z}$ is set to be 30 to get convergent solutions (upper plot).

In the following four figures, Figs. 3–6, a single mass rolling on a beam under different conditions is considered. Fig. 3 shows the deflection at mass (trajectory of mass) vs. the position of mass along the beam due to the influence of geometric imperfection of beam when the mass is set on motion with constant forward force, $\hat{f} = 0.25$. Three different values of initial speed of the

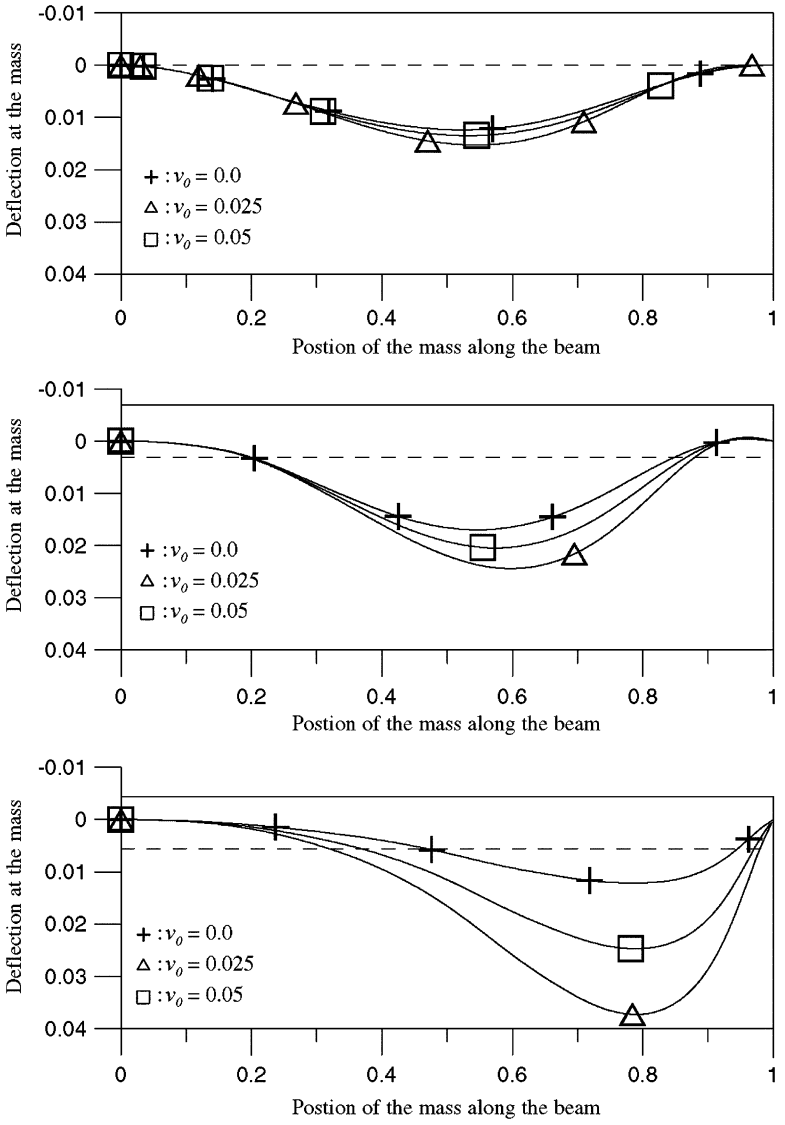

Fig. 3. Deflection at mass vs. the position of mass along the beam due to the influence of geometric imperfection of beam for three different values of initial speed of the mass, $\dot{\xi}(0) = 0.0$ (top plot), 0.25π (middle one), and 0.75π (bottom plot).

mass are chosen; they are $\dot{\xi}(0) = 0.0$ (top plot), 0.25π (middle plot), and 0.75π (lowest plot); other parameters used are $\hat{M} = 0.5$ and $\mu = \hat{k} = 0.0$. Fig. 4 indicates similar information to that shown in Fig. 3, except in this figure the initial speed of the mass is zero ($\dot{\xi}(0) = 0.0$) and the mass is accelerated by three different values of forward thrust, respectively; they are $\hat{f} = 0.25$(top plot), 0.5 (middle one), and 0.75 (bottom plot). Other parameters applied in this figure are $\hat{M} = 0.5$ and $\mu = \hat{k} = 0.0$. Figs. 3 and 4 clearly indicate that the initial curvature of beam plays an important role to the response of the system. In general, the initial imperfection amplifies the amplitude of

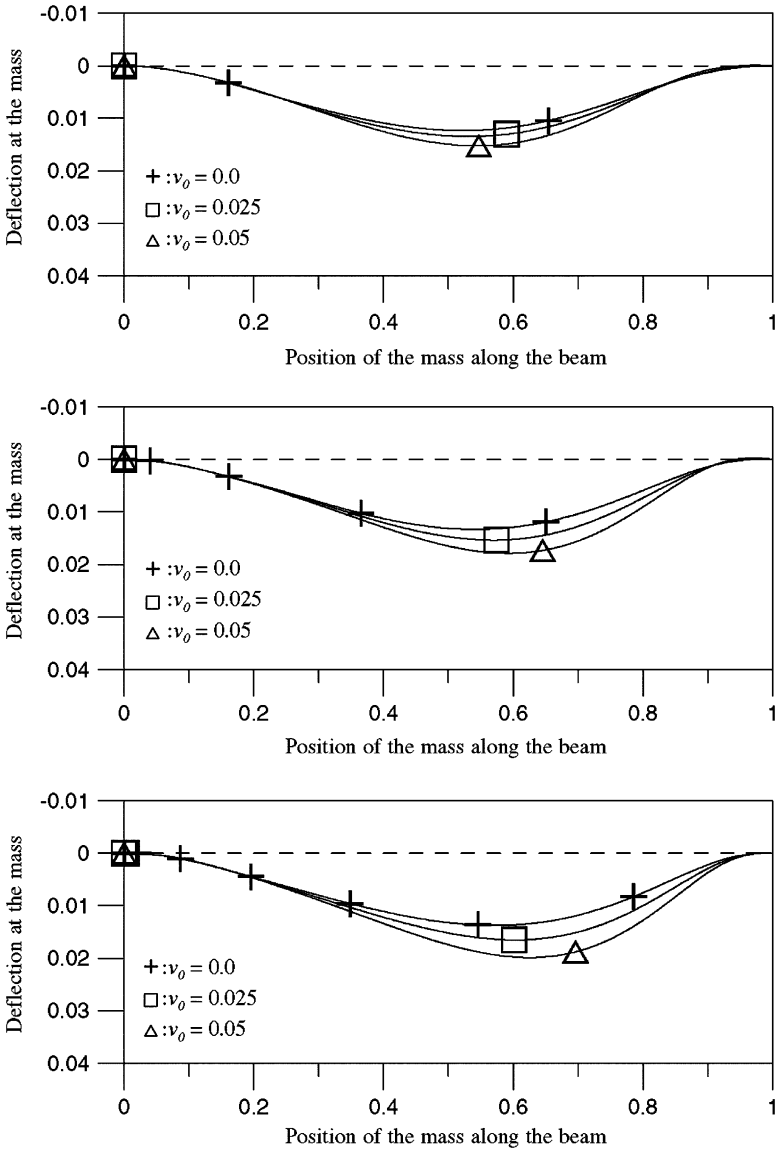

Fig. 4. Deflection at the mass vs. the position of mass along the beam due to the influence of the initial curvature of beam for three different values of forward force, $\hat{f} = 0.25$ (top plot), 0.5 (middle one), and 0.75 (lowest plot).

deflection at mass even if the initial deviation is small. From these two figures, it can be concluded that the enlargement of the amplitude of deflection at mass due to the initial curvature of beam increases with the increase of initial speed and forward thrust of the mass.

As mentioned, the mass can be accelerated by a forward force. Meanwhile, it is capable of reducing speed by applying a reverse force to the mass and/or increasing the friction between the mass and the beam. The friction then can be served as another braking unit of the system. Hence,

the following two figures present the influence of geometric imperfection of beam to the response of the system under the condition when the speed of mass decreases.

Fig. 5 indicates the manner in which the deflection at mass develops as a function of the position of mass along the beam for $\hat{M} = 0.5$, $\mu = \hat{k} = 0.0$, and $\dot{\xi}(0) = 0.5\pi$. Three different values of retard force are selected; those are $\hat{f} = -0.75$ (top plot), -1.0 (center one), and -1.3 (lowest plot). Fig. 6 indicates the same information as does Fig. 5, except in this figure the retard force

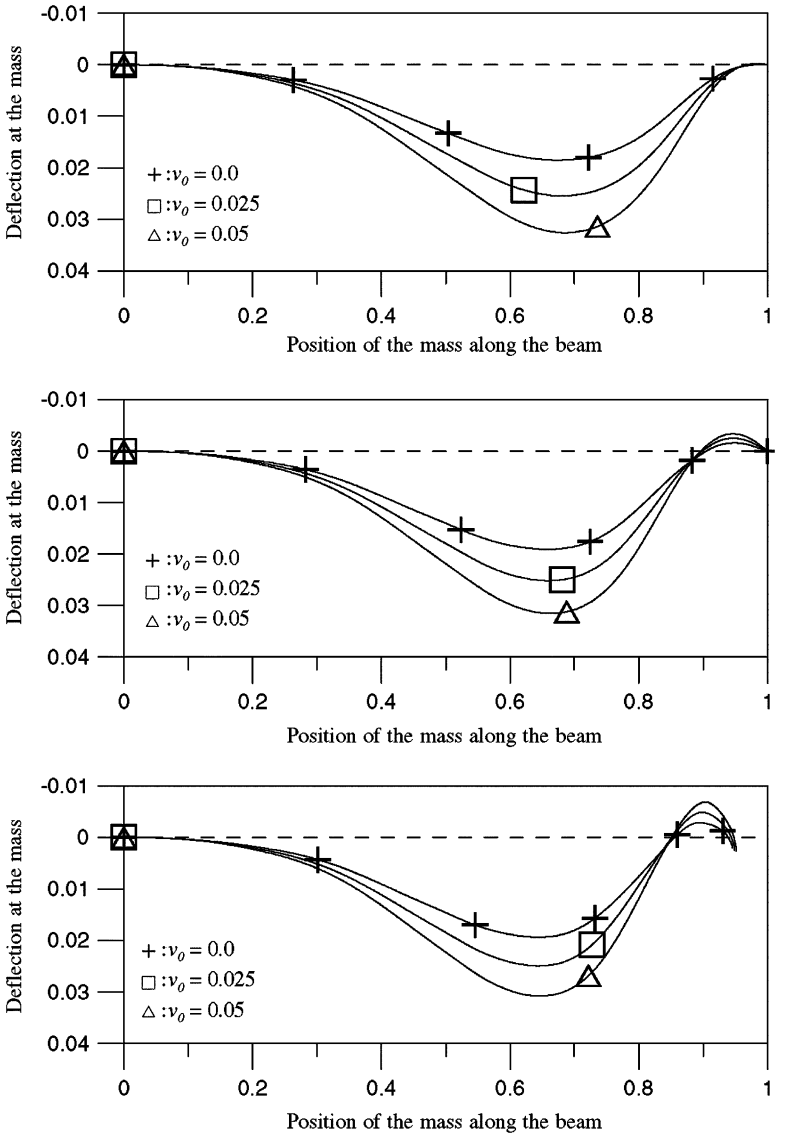

Fig. 5. Deflection at the mass develops as a function of the position of mass along the beam due to the influence of the initial curvature of beam when retard force is applied on the mass. Three different values of retard force are used, $\hat{f} = -0.75$ (top plot), -1.0 (middle one), and -1.3 (lowest plot).

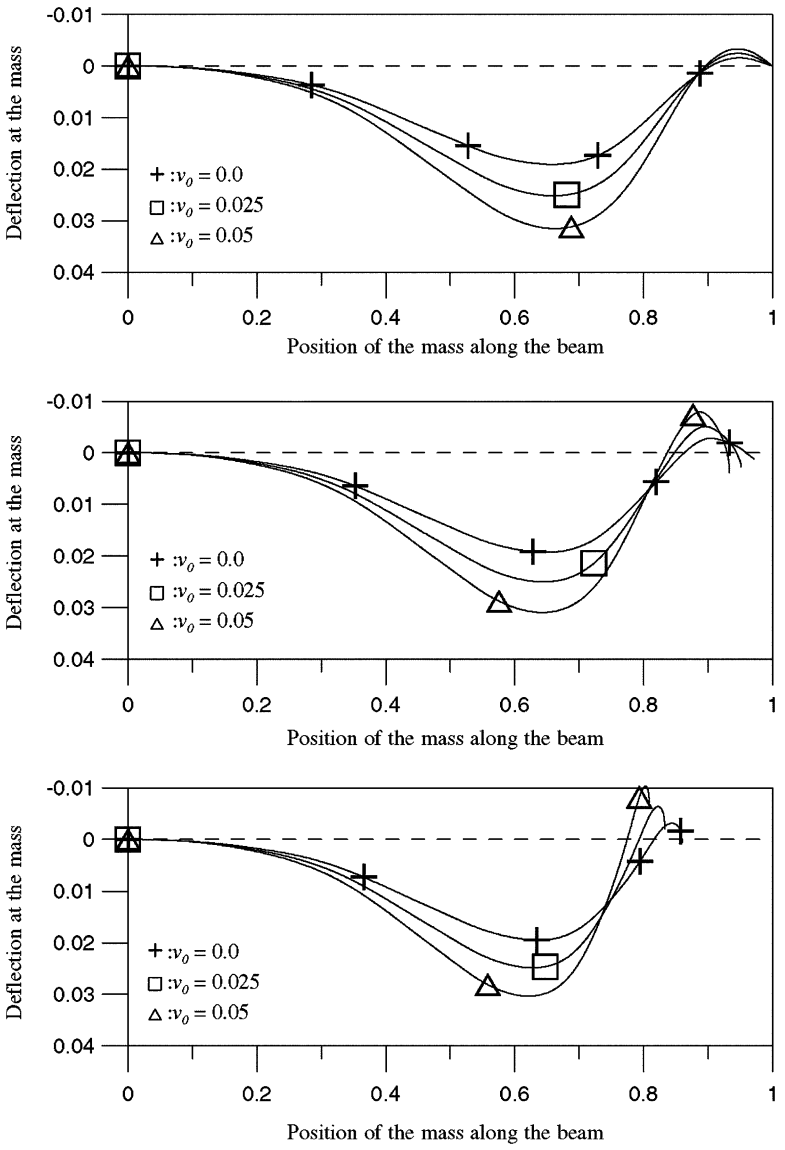

Fig. 6. Deflection at the mass develops as a function of the position of mass along the beam due to the influence of the initial curvature of beam for three different values of the friction μ, $\mu = 0.0$ (top plot), 0.15 (middle one), and 0.3 (lowest plot).

applied on the mass is constant, $\hat{f} = -1.1$, and three different values of the coefficient of friction are chosen; they are $\mu = 0.0$ (top plot), 0.15 (middle one), and 0.3 (floor plot). Other parameters used are $\hat{M} = 0.5$, $\dot{\xi}(0) = 0.5\pi$, and $\hat{k} = 0.0$. The result of these two figures indicates that under certain conditions, negative displacement at mass, which implies the separation of beam and mass, may exist if the mass is going to stop near the right end of the beam. In general, the amplitude of negative displacement increases as the magnitude of retard force and the friction increase. The

result also shows that the geometric imperfection of beam amplifies the amplitude of negative displacement.

Fig. 7 shows a comparison of the deflection profile of beam between a single mass (upper plot) and two masses (lower one) rolling on a straight beam ($\hat{v}_0 = 0$), respectively. Four instant positions of the mass are chosen; for a single mass they are $\xi = 0.2$, 0.5, 0.8, and 1.0; for two masses the four instant positions are selected at the first mass. The parameters used for a single mass are $\hat{M} = 0.5, \hat{f} = 0.1$, $\mu = \hat{k} = 0.0$, and $\dot{\xi}(0) = 0.25\pi$; for two masses the parameters used are $\mu = \hat{k} = 0.0$, $\hat{M}_1 = \hat{M}_2 = 0.25$, $\xi_1 - \xi_2 = 0.5$, $\hat{f}_1 = \hat{f}_2 = 0.1$, and $\dot{\xi}_1(0) = 0.25\pi$. The result indicates that the phenomena produced by a single mass and two masses may be different. As an example, for a single moving mass (upper plot) it is seen that negative displacement occurs when the mass is at the right end of the beam ($\xi = 1.0$). However, for two traveling masses (lower

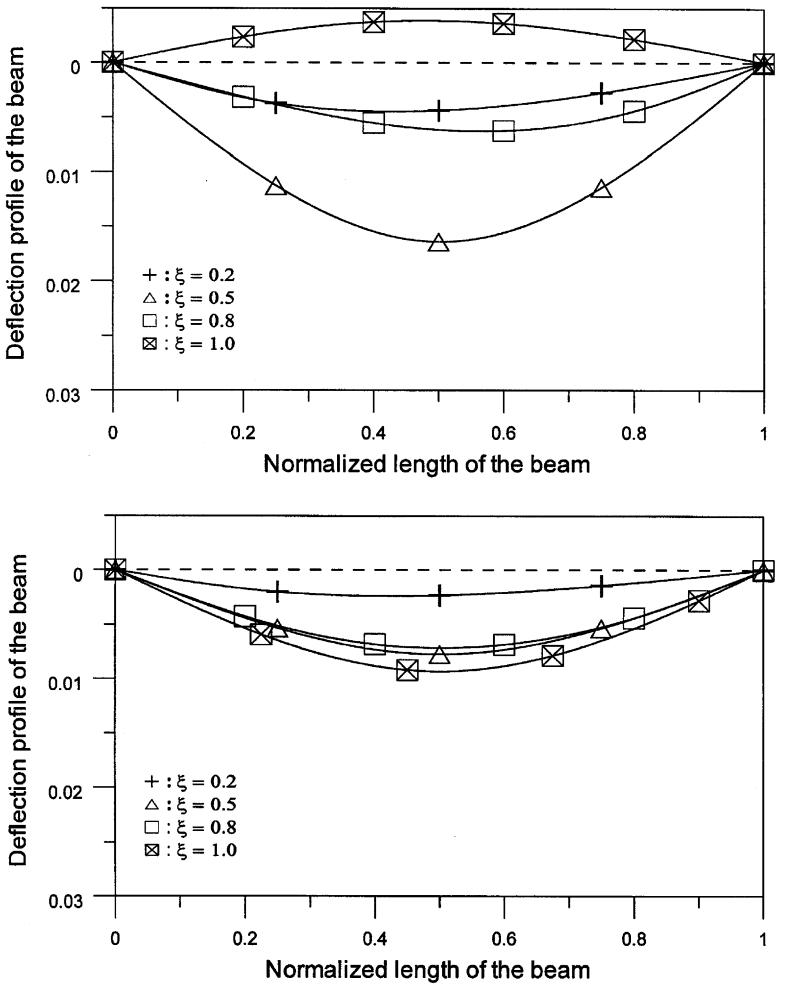

Fig. 7. A comparison of the deflection profile of beam between a single mass (upper plot) and two masses (lower plot) rolling on a straight beam ($v_0 = 0.0$) for four instant positions of the mass. The four instant positions are: $\xi = 0.2$, 0.5, 0.8, and 1.0. For the lower plot, the four instant positions are measured at the first mass.

plot), not only no negative displacement is found, but also the amplitude of deflection of beam is largest when the first mass travels to the right end of the beam ($\xi_1 = 1.0$). Although, this is expected because under this condition, the second mass is just at the midpoint of the beam ($\xi_1 - \xi_2 = 0.5$), however, it is seen that the phenomena generated by a single mass and two masses may be different. Hence, in the following, a beam–mass system carrying two moving masses will be studied.

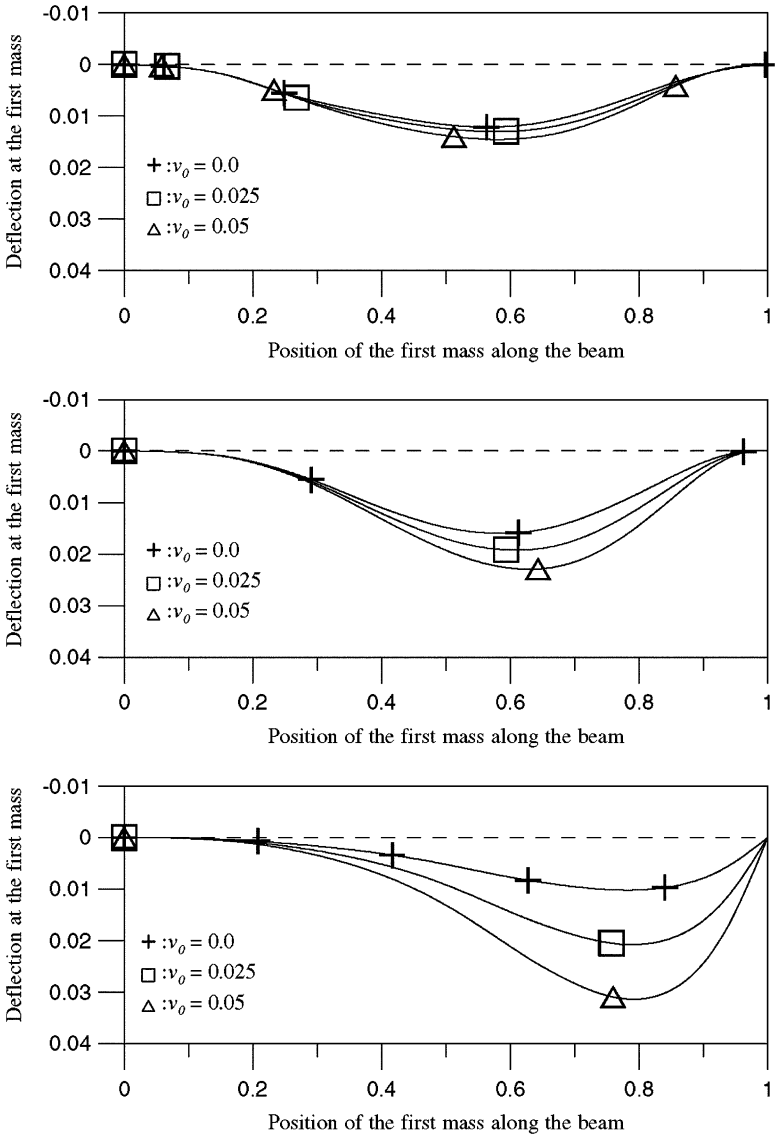

Fig. 8. Deflection at the first mass vs. the position of the first mass along the beam due to the influence of geometric imperfection of beam for three different values of initial speed of the mass, $\xi(0) = 0.0$ (top plot), 0.25π (middle one), and 0.75π (bottom plot).

Fig. 8 shows the manner in which the deflection at the first mass is plotted as a function of the position of the first mass along the beam. Three different values of initial speed of the first mass are chosen; they are $\dot{\xi}_1(0) = 0.0$ (top plot), 0.25π (middle one), and 0.75π (lowest plot). Other parameters used are $\hat{M}_1 = \hat{M}_2 = 0.25$, $\hat{f}_1 = \hat{f}_2 = 0.25$, $\hat{k} = \mu = 0$, and $\xi_1 - \xi_2 = 0.1$. Fig. 9 indicates similar information to that shown in Fig. 8, except in this figure $\dot{\xi}_1(0) = 0.75\pi$ and three different values of the distance between the two masses are chosen, $\xi_1 - \xi_2 = 0.1$ (top one), 0.3

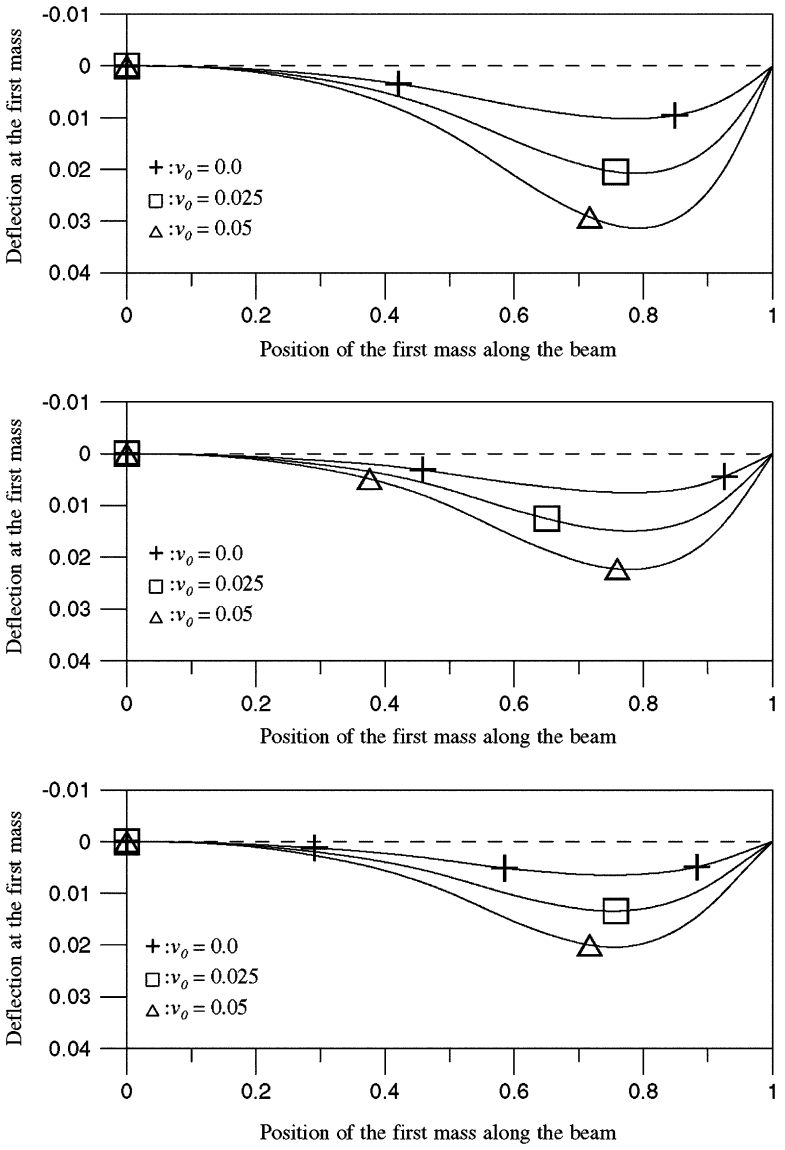

Fig. 9. Deflection at the first mass vs. the position of the first mass along the beam due to the influence of geometric imperfection of beam for three different values of the distance between the two masses, $\xi_1 - \xi_2 = 0.1$ (top plot), 0.3 (middle one), and 0.5 (bottom plot). The initial speed is $\dot{\xi}_1 = 0.75\pi$.

(center plot), and 0.5 (bottom one). The result indicates that the deflection at mass is significantly affected by the initial speed of the mass and the initial curvature of beam. The amplitude of deflection at the first mass increases with the increase of the initial speed of the mass and the initial deviation of beam.

Figs. 10 and 11 illustrate the influence of geometric imperfection of beam to the response of the system at the first mass when the speed of mass decreases. In Fig. 10, the parameters used are $\mu = \hat{k} = 0.0$, $\hat{M}_1 = \hat{M}_2 = 0.25$, $\hat{f}_1 = \hat{f}_2 = -1.3$, $\dot{\xi}_1(0) = 0.5\pi$, and three different values of the

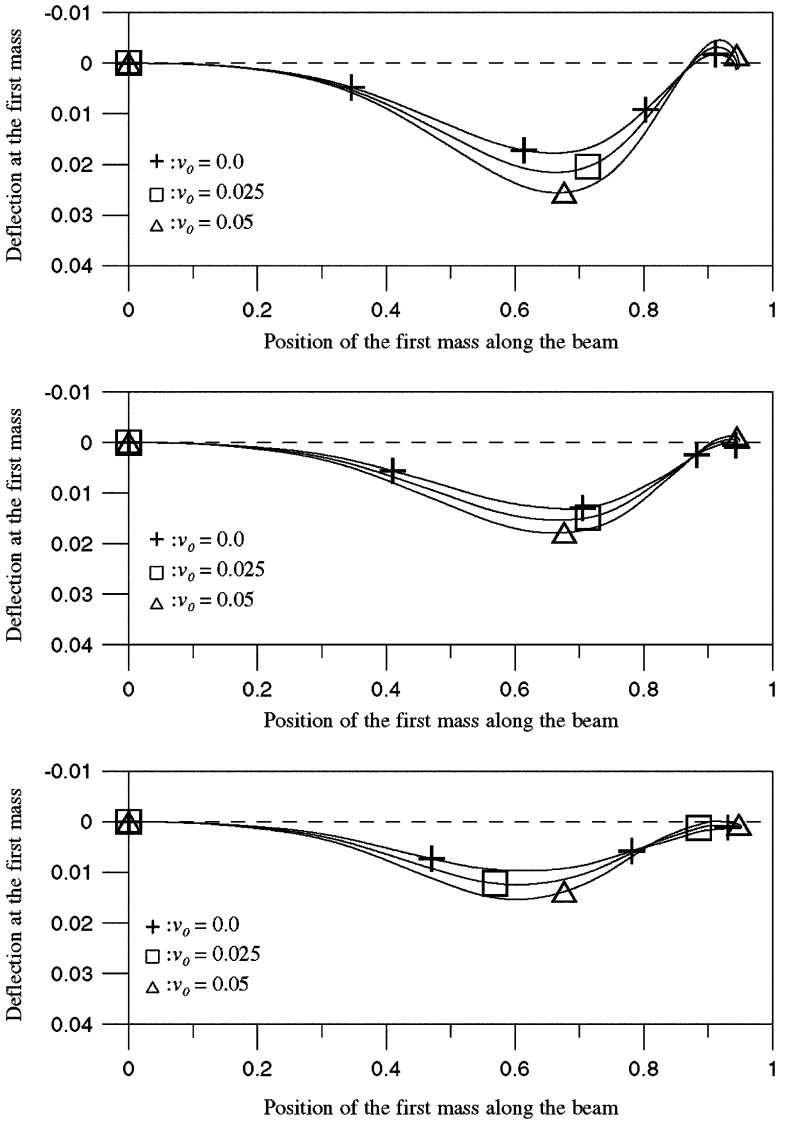

Fig. 10. The influence of geometric imperfection of beam to the deflection at the first mass when retard force is applied on the mass ($\hat{f}_1 - \hat{f}_2 = -1.3$). Three different values of $\xi_1 - \xi_2$ are used, $\xi_1 - \xi_2 =$ 0.1 (top plot), 0.3 (middle one), and 0.5 (lowest plot). The initial speed is $\dot{\xi}_1(0) = 0.5\pi$.

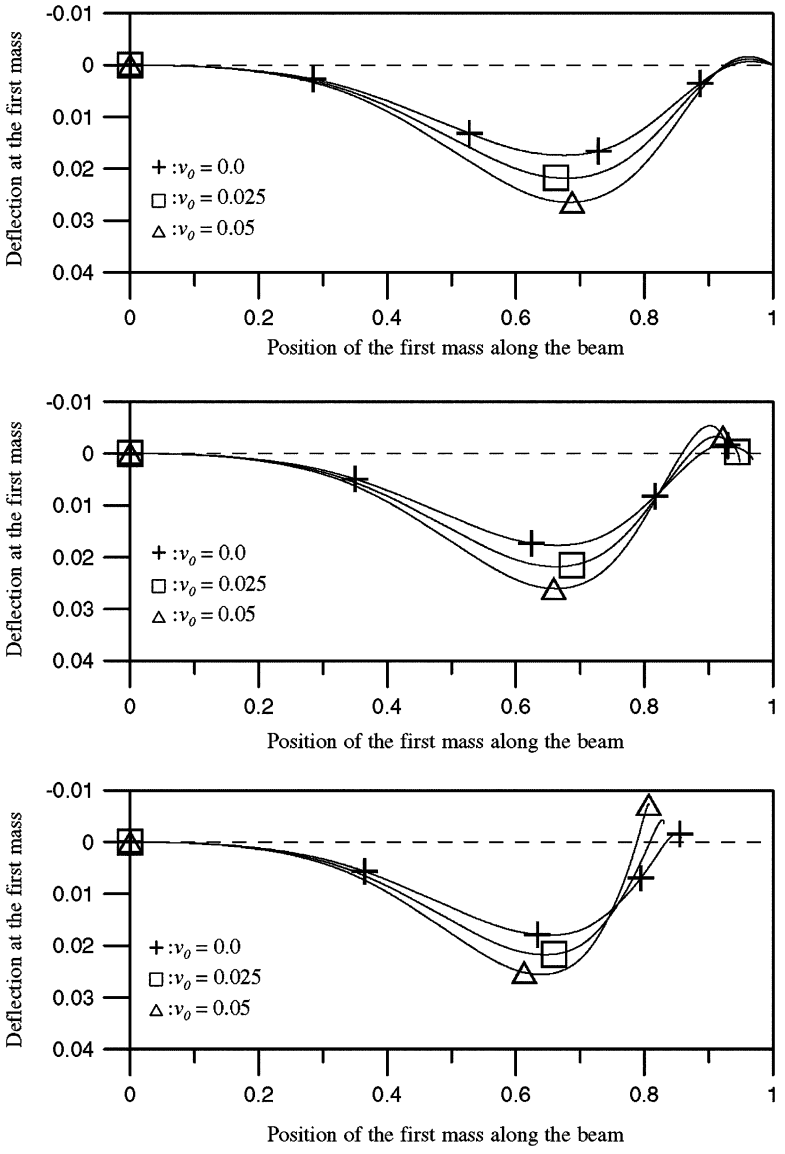

Fig. 11. Deflection at the first mass vs. the position of the first mass along the beam due to the influence of geometric imperfection of beam when the speed of mass decreases. Three different values of the friction are selected, $\mu = 0.0$ (top plot), 0.15 (middle one), and 0.3 (bottom plot).

distance between the two masses; they are $\xi_1 - \xi_2 = 0.1$ (top plot), 0.3 (middle one) and 0.5 (bottom plot). In Fig. 11, the parameters selected are $\xi_1 - \xi_2 = 0.1$, $\hat{k} = 0.0$, $\hat{M}_1 = \hat{M}_2 = 0.25$, $\hat{f}_1 = \hat{f}_2 = -1.1$, $\dot{\xi}_1(0) = 0.5\pi$, and three different values of the friction; they are $\mu = 0.0$ (top plot), 0.15 (middle one), and 0.3(bottom plot). It clearly indicates that the retard force and the friction can serve as a simulated braking system and can be used to bring the moving masses to a

halt at desired point on the beam. In addition, it is interesting to note that the friction and the initial curvature of beam may amplify the amplitude of negative displacement at the first mass.

The comparison of the deflection at the first mass and the second mass is given in Figs. 12 and 13. In Fig. 12, the lower plot presents the deflection at the first mass vs. the position of the first mass along the beam. The lower diagram indicates the deflection at the second mass vs. the position of the second mass along the beam. The parameters used are $v_0 = 0$, $\mu = \hat{k} = 0.0$, $\dot{\xi}_1(0) = 0.5\pi$, $\hat{M}_1 = \hat{M}_2 = 0.4$, $\xi_1 - \xi_2 = 0.2$, and three different values of the retard force, $\hat{f}_1 = \hat{f}_2 = -0.5$, -1.0 and -1.5. Fig. 13 illustrates the effect of elastic foundations to the deflection at the masses. This figure shows the same information as does Fig. 12, except in the figure three different values of the stiffness of elastic foundation are selected; they are $\hat{k} = 0$, 100, and 200. The retard force applied on the masses is $\hat{f}_1 = \hat{f}_2 = -1.0$.

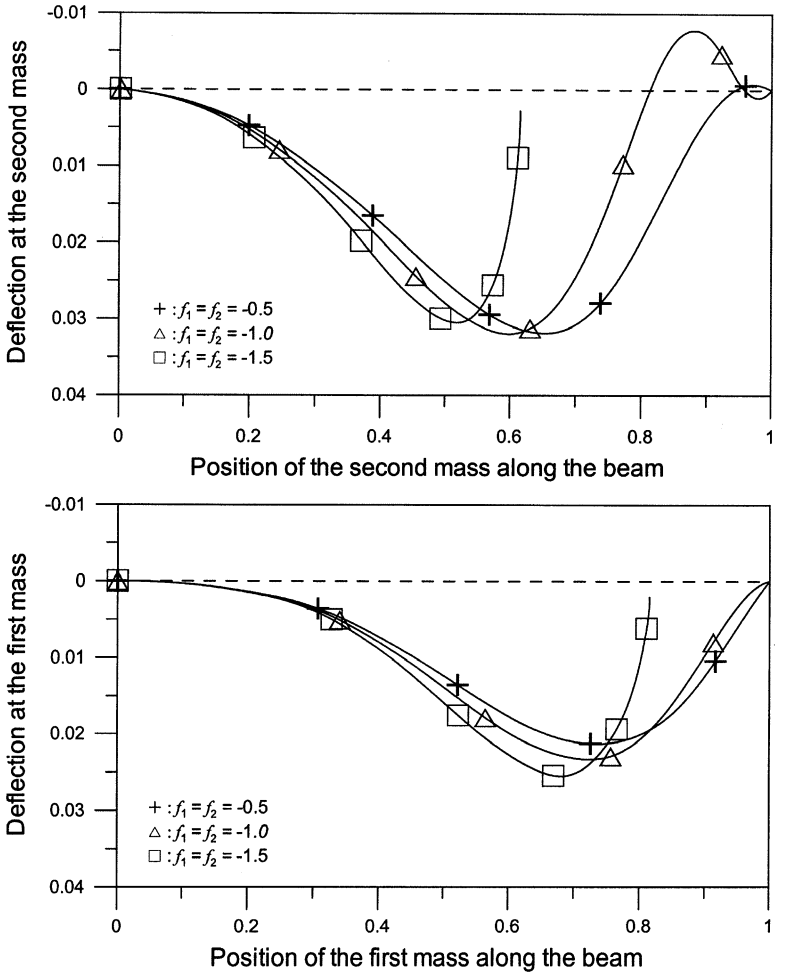

Fig. 12. Deflection at the first mass (lower plot) and at the second mass (upper one) rolling on a straight beam ($v_0 = 0.0$) for three different values of retard force. They are $\hat{f}_1 = \hat{f}_2 = -0.5, -1.0$, and -1.5. Other parameters used are $\dot{\xi}_1(0) = 0.5\pi$, $\hat{M}_1 = \hat{M}_2 = 0.4$, $\mu = 0.0$, and $\xi_1 - \xi_2 = 0.2$.

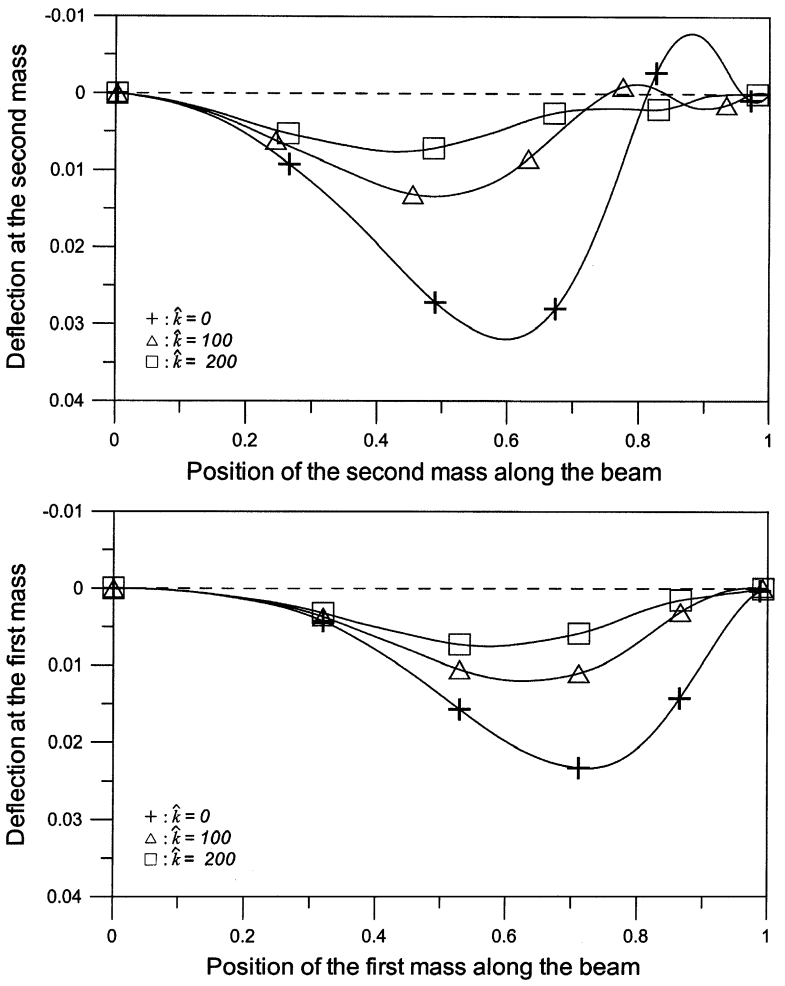

Fig. 13. Deflection at the first mass (lower plot) and at the second mass (upper one) rolling on a straight beam ($v_0 = 0.0$) for three different values of elastic foundation. They are $\hat{k} = 0$, 100, and 200. Other parameters used are $\dot{\xi}_1(0) = 0.5\pi$, $\hat{M}_1 = \hat{M}_2 = 0.4$, $\hat{f}_1 = \hat{f}_2 = -1.0$, $\mu = 0.0$, and $\xi_1 - \xi_2 = 0.2$.

From Figs. 12 and 13, it is found that the dynamic behaviors at the first mass and the second mass are generally different. As an example, when the first mass is near the right end, no negative displacement is found. This is expected since the second mass is still riding on the beam when the first mass is close to the right end. The result of Fig. 13 also indicates that, as expected, the increase of the foundation stiffness diminishes the amplitude of deflection at the masses.

4. Conclusions

In this study, the transient dynamics of multiple accelerating/decelerating masses traveling along an initially curved beam are studied. In the modeling, the coupled equations of motion of

multiple moving masses rolling on a beam with initial curvature are derived. In the numerical analysis, the transient dynamics of a beam–mass system carrying one and two traveling masses traveling on an initially curved beam are studied.

Result of present study shows that the initial curvature of a beam can result significant effects to the dynamics of the system even if the initial imperfection of the beam is small. In general, the initial imperfection of beam amplifies the amplitude of vibration of the system. It can be concluded that for accelerating case, the magnification of the amplitude of response at mass due to the initial deviation of beam grows with the increase of initial speed and forward force. For decelerating condition, the growth of the deflection at mass caused by the initial imperfection of beam increases with the increase of initial speed, applied retard force, and the friction between the mass and the beam.

In this study, the traveling mass may reduce its speed by applying a retard force and/or increasing the friction between the mass and the beam. The retard force and the friction then can serve as a simulated braking system. Under certain conditions, negative displacement at mass may occur if the mass approaches to stop near the right end of the beam. The result indicates that the amplitude of negative displacement at mass increases with the increase of the initial curvature of beam.

In addition, under the condition when multiple traveling masses is considered, the response of the system at different masses are distinct. As shown in Figs. 12 and 13, negative displacement at the second mass occurs when the second mass is near the right end of the beam. However, no negative displacement at the first mass is observed.

Appendix

$$\mathbf{M} = [M_{jn}], \quad M_{jn} = \delta_{jn} + 2\sum_{i=1}^{m} \hat{M}_i \hat{S}_{ijn}(\xi_i),$$

$$\mathbf{N}_i = [N_{ijn}], \quad N_{ijn} = 4\hat{M}_i R_{ijn}(\xi_i),$$

$$\mathbf{K}_1 = [K_{1jn}], \quad K_{1jn} = ((j\pi)^4 + \hat{k})\delta_{jn} - 2\sum_{i=1}^{m} \hat{M}_i \hat{f}_i R_{ijn}(\xi_i),$$

$$\mathbf{K}_{2i} = [K^i_{2jn}], \quad K^i_{2jn} = 2\hat{M}_i R_{ijn}(\xi_i),$$

$$\mathbf{K}_{3i} = [K^i_{3jn}], \quad K^i_{3jn} = -2\hat{M}_i S_{ijn}(\xi_i),$$

$$\tilde{\mathbf{c}}_i = (\tilde{C}_{ij}), \quad \tilde{C}_{ij} = 2\hat{M}_i v_0 R_{ij1}(\xi_i),$$

$$\tilde{\mathbf{s}}_i = (\tilde{S}_{ij}), \quad \tilde{S}_{ij} = -2\hat{M}_i v_0 S_{ij1}(\xi_i),$$

$$\mathbf{h} = (h_j), \quad h_j = 2\sum_{i=1}^{m} \hat{M}_i[\hat{g}\hat{S}_{ij}(\xi_i) + \hat{f}_i v_0 R_{ij1}(\xi_i)],$$

$$\mathbf{s}_i = (S_{in}), \quad S_{in} = S_{in}(\xi_i) = (n\pi)^2 \sin n\pi\xi_i = (n\pi)^2 \hat{S}_{in}(\xi_i),$$

$$\mathbf{c}_i = (C_{in}), \quad C_{in} = C_{in}(\xi_i) = (n\pi)\cos n\pi\xi_i,$$

$$\mathbf{d}_i = -\hat{g}(\hat{S}_{in}),$$

$$\mathbf{e}_i = -\mu(C_{in}),$$
$$p_i(\xi_i, \mathbf{y}) = \mu \mathbf{s}_i^{\mathrm{T}} y, \quad \mathbf{s}_i = (S_{in}), \quad S_{in} = S_{in}(\xi_i) = (n\pi)^2 \sin n\pi\xi_i = (n\pi)^2 \hat{S}_{in}(\xi_i),$$
$$q_i(\xi_i, \mathbf{y}) = -2\mu_i \mathbf{c}_i^{\mathrm{T}} \dot{\mathbf{y}}, \quad \mathbf{c}_i = (C_{in}), \quad C_{in} = C_{in}(\xi_i) = (n\pi)\cos n\pi\xi_i,$$
$$f_i^* = (\hat{f}_i - \mu\hat{g}) + \hat{g} v_0 C_{i1}.$$

References

[1] C.R. Steele, The finite beam with a moving load, *Journal of Applied Mechanics* 34 (1967) 111–118.
[2] C.R. Steele, The Timoshenko beam with a moving load, *Journal of Applied Mechanics* 35 (1968) 481–488.
[3] E.C. Ting, J. Genin, J.H. Ginsberg, A general algorithm for moving mass problems, *Journal of Sound and Vibration* 33 (1974) 49–58.
[4] U. Lee, Separation between the flexible structure and the moving mass sliding on it, *Journal of Sound and Vibration* 209 (1998) 867–877.
[5] G.G. Adams, Critical speeds and the response of a tensioned beam on an elastic foundation to repetitive moving loads, *International Journal of Mechanical Sciences* 37 (1995) 773–781.
[6] Y.M. Wang, The dynamic analysis of a beam–mass system due to the occurrence of two-component parametric resonance, *Journal of Sound and Vibration* 258 (2002) 951–967.
[7] A.V. Kononov, R. de Borst, Instability analysis of vibrations of a uniformly moving mass in one and two-dimensional elastic systems, *European Journal of Mechanics A/Solids* 21 (2002) 151–165.
[8] M. Mofid, M. Shadnam, On the response of beams with internal hinges, under moving mass, *Advances in Engineering Software* 31 (2000) 323–328.
[9] Y.M. Wang, The dynamical analysis of a finite inextensible beam with an attached accelerating mass, *International Journal of Solids and Structures* 35 (1998) 831–854.
[10] A. Yavari, M. Nouri, M. Mofid, Discrete element analysis of dynamic response of Timoshenko beams under moving mass, *Advances in Engineering Software* 33 (2002) 143–153.
[11] L. Fryba, *Vibration of Solids and Structures Under Moving Loads*, Thomas Telford, London, 1999.
[12] R.S Ayre, L.S. Jacobson, C.S. Hsu, Transverse vibration of one- and two-span beams under the action of a moving mass load, *Proceedings of the First National Congress of Applied Mechanics*, 1951, pp. 81–90.
[13] S. Park, Y. Youm, Motion of a moving elastic beam carrying a moving mass—analysis and experimental verification, *Journal of Sound and Vibration* 240 (2001) 131–157.